Thermodynamic and elastic properties of a many-body model for simple oxides

Amotz Agnon* and M. S. T. Bukowinski
Department of Geology and Geophysics, The University of California at Berkeley, Berkeley, California 94720
(Received 13 October 1989)

Many-body effects in the binding energy of oxides can be incorporated efficiently in empirical Hamiltonians by including terms that describe the response of the ionic charge density to the crystalline environment. It is assumed that the effect of the ionic response on interionic interactions is completely characterized by the dependence of the ionic radius on the crystal field, which in turn is given by the positions of all the ions in the system. The model is particularly suitable for oxides, where the field is necessary to stabilize the O^{2-} ion. This scheme has allowed *ab initio* electron-gas models to predict elasticity and phase transitions in oxides. Here we propose simple parametric expressions for the dependence of the ionic radius on the crystal field, and the dependence of the energy on the former. By parametrizing the Hamiltonian, and solving for harmonic phonon spectra without approximations, we obtain accurate volume-dependent thermodynamic properties at the experimentally accessible range of pressure and temperature. Predictions of thermoelastic properties at conditions beyond experimental capabilities are readily obtained. Of particular interest is our finding that the sensitivity of the compressibility to temperature decreases significantly at high compressions. Reduction of thermal effects at high pressures is plausible from a theoretical standpoint. However, the only physical manifestation of our prediction comes from the geophysical data on the Earth's interior. Seismic studies find that the transverse-acoustic velocity in the Earth's oxide mantle is significantly more sensitive to temperature than the longitudinal velocities. Partial melting has been suggested for reconciling this observation with the behavior of relevant minerals under laboratory conditions. Our results support the alternative conjecture, that the relative insensitivity of the longitudinal waves to temperature is a characteristic of oxygen-bearing minerals at high pressure.

I. INTRODUCTION

Close-packed oxides are distinguished from other ionic solids in that the electron density of the valence electrons around the anion depends strongly on the crystal environment.[1,2] This feature poses a difficulty to traditional atomistic descriptions that have been instrumental in the study of cohesive and vibrational properties of halides.[3] While progress in first principles and *ab initio* studies of oxides is encouraging,[1,4–6] parametric models have a considerable appeal in investigations of complex structures. This approach offers economy in computation, while it may clarify the physical picture, often blurred by the details of the orbital structure. In addition, experimental data constrain the calculations and warrants accuracy in predictions. The investigation of materials and geophysically important phases under conditions that are difficult to reproduce experimentally will clearly benefit from simple and reliable parametric models.

A number of adjustments to the ionic picture adapted from the halides have been proposed. As opposed to pairwise additive ion-ion interaction schemes for calculating the crystal potential, these models include many-body terms. The breathing-shell model[7] incorporates isotropic deformation of the valence shell in response to the short-range repulsion. A different many-body approach is offered by charge exchange models[8] that consider corrections to the Madelung energy due to the extensive overlap of oxygen and its neighbors. In these models the many-body effects depend only on the distances from neighboring ions. Thus the interactions between the poorly bound valence shell and the long-range field has been left out.

The premise of the present study is that the sensitivity of the valence states to the crystal configuration comprises the major contribution to noncentral forces in oxides. This suggests a parametric description, where the adjustments in the valence band are represented by the deformation of the ionic charge-density distribution. The principal characteristics of the charge density in the ionic picture are the total ionic charge and its radial extent, represented by an ionic radius. The innovation in the present approach is in letting the effective ionic radius vary dynamically, responding to changes in the environment. In a previous paper[9] we have shown that a simple parametric model can capture the many-body nature of bonding in a transparent way by allowing the ionic radius of oxygen to vary as a function of the crystal field. The model reproduced the elastic constants of the alkaline-earth oxides, and accurately predicted pressure derivatives of elastic constants. Moreover, the calculated pressures at which transformations from the $B1$ (NaCl-type) to $B2$ (CsCl-type) structures occur in the cubic alkaline-earth oxides were in good agreement with experiment. In this paper we apply the model to the study of thermodynamic properties of these oxides, and to predictions of thermoelasticity at high compression.

The physical picture that underlies the model has been

developed in electron-gas *ab initio* studies.[10] Postulating that the dependence of the valence band on volume reflects a sensitivity of the charge distribution to the crystal field; this scheme enabled quantitative modeling of a variety of ground-state properties.[6,11,12] Most notable are the successful predictions of the sign of the deviation from Cauchy relation, and predictions of phase transformations and pressure derivatives of shear moduli in satisfactory agreement with experiment. These features suggest that the many-body interactions are reasonably represented.

In these electron-gas models the charge-density distribution is taken as a superposition of the component spherical ion's charge densities, where O^{2-} needs to be stabilized by an external potential that simulates the crystal field. This stabilization is in the foundation of the present approach. Here it is the variable ionic radius that emulates the deformable valence orbitals. In Sec. II we outline the utilization of this concept in parametric models.

Section III applies the interatomic potential model to macroscopic properties. The dynamic matrices derived from our original model are irregular at the Brillouin-zone center.[13] In the present formulation we avoid this anomaly by a careful redefinition of the potential that stabilizes O^{2-}. This modification does not affect the dynamic matrices for infinite wavelengths, and hence the static elastic constants and phase stability results are unchanged. The present treatment is thus a generalization of the original one, that was restricted to point-inversion invariant configurations and transformations. Section III B discusses the modification in the definition of the stabilizing potential, and Appendix B outlines the corrections in the dynamic matrices.

We describe the results of our calculations in Sec. IV. It is of interest to compare the predictions of physical models with inferences from seismology, which provides the most extensive data on the equation of state and elasticity of compressed hot minerals. The pressures inside the Earth are in the megabar range with temperatures of a few thousand degrees.[14] Current interpretations of the seismic data suggest that the behavior of certain thermoelastic parameters differ markedly from our experience at laboratory conditions.[15] This offers an opportunity to test our understanding and our models of bonding in condensed matter. In Sec. V we compare our predictions with some inferences derived from seismic data in extreme pressures and temperatures.

II. MANY-BODY PARAMETRIC HAMILTONIAN

As in traditional parametric ionic models[3] the leading contributions to the binding energy are the Madelung and short-range repulsion terms. The short-range repulsion between two neighbors, however, depends on the positions of all the ions. We accomplish this by assigning an internal state (R) of energy $S(R)$ to O^{2-}. This internal degree of freedom depends on the crystal configuration, and controls the interaction of O^{2-} with a given neighbor. This degree of freedom is assumed to be represented by an effective ionic radius.

The crystal potential is thus given by

$$\Phi=\tfrac{1}{2}\sum_{m,m',j,j'}{}' z_j z_{j'}\left|x\begin{bmatrix}m & m'\\ j & j'\end{bmatrix}\right|^{-1}+\tfrac{1}{2}\sum_{m,m',j,j'}{}'\phi\left(\left|x\begin{bmatrix}m & m'\\ j & j'\end{bmatrix}\right|,R\begin{bmatrix}m\\ j\end{bmatrix},R\begin{bmatrix}m'\\ j'\end{bmatrix}\right)+\sum_{m,j}S\left(R\begin{bmatrix}m\\ j\end{bmatrix}\right) \tag{1}$$

The first term on the right-hand side of Eq. (1) is the long-range electrostatic energy due to a lattice of point charges. x is a lattice vector between two ions of types j and j', at unit cells m and m' respectively. Z_j is the ionic charge of j and the primed summation symbol indicates that the self-interaction terms are omitted. The second term arises from overlap between neighboring ions. ϕ is a function of the internuclear spacing, as well as of the states of the overlapping ions. The dependence of R on the crystal configuration distinguishes the short-range interactions in the present model from traditional parametric models. The last sum on the right-hand side of (1) is extended over all deformable ions.

We assume that the short-range repulsion is represented by

$$\phi\left(x\begin{bmatrix}l & l'\\ k & k'\end{bmatrix},R\begin{bmatrix}l\\ k\end{bmatrix},R\begin{bmatrix}l'\\ k'\end{bmatrix}\right)=b\left[\frac{R\begin{bmatrix}l\\ k\end{bmatrix}+R\begin{bmatrix}l'\\ k'\end{bmatrix}}{x\begin{bmatrix}l & l'\\ k & k'\end{bmatrix}}\right]^{n_{kk'}}, \tag{2}$$

where b is a scalar with dimension of energy and $R\binom{l}{k}$ is the effective radius of ion type k at unit cell l. The exponent is given by $n_{kk'}=n_k+n_{k'}$, where n_k is unique to ion k. The effect of the environment on R_{ox} (subscript denotes O^{2-}) is mediated through the crystal field, which acts to stabilize the unbound $2P$ orbitals. The dependence of R_{ox} on the crystal field Δ has the form:

$$R\left(\Delta\begin{bmatrix}l\\ k\end{bmatrix}\right)=R_k^0+\frac{Q_k}{\Delta\begin{bmatrix}l\\ k\end{bmatrix}}. \tag{3}$$

Q is a positive number with the dimension of charge. In the absence of a stabilizing field, $\Delta\binom{l}{k}=0$, the right-hand side of (3) is infinite, reflecting the instability of O^{2-} as a free ion. As the lattice is compressed, $\Delta\binom{l}{k}$ increases and thus diminishes the ionic radius, as we stipulate. R_k^0 is the limit where an infinite stabilizing potential is applied.

The self-energy of O^{2-} is composed of the kinetic energy of its electrons, and of electron-electron and electron-nucleus Coulomb interactions. For a free-electron gas, the kinetic energy varies as the square of the inverse dimension of the system, while the potential energy scales as its inverse. This suggests for the self-energy the simple

approximation

$$S\left[\Delta\begin{bmatrix} l \\ k \end{bmatrix}\right]=\sigma_k\left[\frac{1}{2}\left[\frac{r_k^s}{R\begin{bmatrix} l \\ k \end{bmatrix}}\right]^2-\frac{r_k^s}{R\begin{bmatrix} l \\ k \end{bmatrix}}\right], \quad (4)$$

where $R\begin{pmatrix} l \\ k \end{pmatrix}$ is the ionic radius [Eq. (3)], r_k^s is the ionic radius at which the self-energy is a minimum, and σ has the dimension of energy. Slater[16] has invoked general scaling arguments to suggest that these dependencies on dimension are not limited to uniform electron gas, and may effectively account for correlations.

The explicit dependence of the self-energy on the repulsive radius $R\begin{pmatrix} l \\ k \end{pmatrix}$ (4) results in coupling among the self-energy, crystal configuration, and overlap energy. As the crystal is compressed, $R\begin{pmatrix} l \\ k \end{pmatrix}$ decreases so as to diminish the repulsive energy. However, since the self-energy increases, the ion acquires a radius for which the resulting short-range forces balance the Coulomb forces.

III. THERMOELASTICITY

A. Homogeneous deformation and lattice statics

The stabilizing field Δ is composed of the long-range point ionic potential as well as short-range contributions from electron overlap. At low pressures the overlap is small and the long-range Madelung potential dominates. To first order, Δ scales like the long-range electrostatic potential at the lattice point. Accordingly, we replace $\Delta\begin{pmatrix} l \\ k \end{pmatrix}$ in (3) by the Madelung potential $P\begin{pmatrix} l \\ k \end{pmatrix}$:

$$\Delta\begin{bmatrix} l \\ k \end{bmatrix}=P\begin{bmatrix} l \\ k \end{bmatrix}=\sum_{l',k'} z_{k'}\left|x\begin{bmatrix} l & l' \\ k & k' \end{bmatrix}\right|^{-1}. \quad (5)$$

This results in a static Hamiltonian (1) that, apart from the form of the energy functionals (2) and (4), is formally identical to the potential-induced breathing (PIB) (Ref. 6) and Coulomb-stabilized modified electron gas[12,10] models. In an earlier paper[9] we have shown the utility of this approximation in calculating elastic constants and phase transition pressure for the cubic alkaline-earth oxides.

The parameters of the model are determined by fitting the analytic expressions for the elastic constants (Appendix A) to our data. We use only data from the low-pressure $B1$ (NaCl-structure) phases of the alkaline-earth oxides. In fitting the parameters we have attempted to minimize the number of parameters that are unique to each compound. We determine the common parameters for the series from the elasticity of CaO. CaO affords a direct measure of the non-central-force part in the Hamiltonian: the observed second-order elastic constant C_{12} differs significantly from C_{44}. Except for vibrational contributions, this difference arises from the different response of $R(\Delta\begin{pmatrix} l \\ k \end{pmatrix})$ of O^{2-} to the distortions that correspond to these elastic constants (Appendix A). In addition, the equation of state of CaO is well characterized, both experimentally[17] and theoretically.[2,4,18] The four cation specific parameters in each of the remaining compounds are determined by fits to the equilibrium lattice constants and three elastic constants.

TABLE I. Model parameters. Cation-independent parameters: $R_{ox}=0.902\,67$ bohr; $Q=0.635$, $n_{ox}=5.341$; $b=0.1864$ hartree.

	R_c (bohr)	σ (hartree)	R_s (bohr)	n_c
MgO	1.449	5.040	2.0200	2.740
CaO	1.743	8.004	2.0010	3.525
SrO	1.893	9.507	2.0295	3.840
BaO	1.979	13.42	2.0490	3.927

In a preliminary study we have modeled the elasticity and equations of states of the alkaline-earth oxides with nearest-neighbor short-range interactions only.[9] The model that represented room pressure elasticity data accurately and successfully predicted high-pressure shear moduli and phase transformations. However, in the nearest-neighbor model, where we are fitting compressional data, the short-range forces between unlike ions absorb the effect of the missing longer bonds. The resulting force constants give rise to overly high optical frequencies, which are controlled by nearest-neighbor short-range forces. To allow for this we have included second-nearest-neighbor interactions in the present treatment. The resulting parameters are listed in Table I.

B. Lattice dynamics of Coulomb stabilized ions

The application of (5) to lattice dynamics results in irregular expressions for longitudinal modes at the Brillouin-zone center.[13] Uniform electric fields that are induced by phonons shift the potential Δ, and cause "breathing" of the ionic charge density.[11] This response is unphysical, since a spherical charge deformation cannot interact with a uniform field. The spurious effect did not appear in the static calculations (Ref. 9) due to the maintenance of inversion symmetry, and thus, the mutual cancellation of polarizing fields at ionic sites. Here we introduce a correction to the model, explicitly eliminating uniform fields from the stabilizing field (5). Care is taken to leave the model for the static case unchanged. We thus preserve the physics and accomplishments of the static model, but relax the requirement on inversion symmetry.

The field of a modulated dipole lattice can be factored out of the dynamical matrix.[13] This field is proportional to $\Theta_\alpha(k,j;\mathbf{q})=\sum'_m e^{-i\mathbf{q}\cdot\mathbf{x}(m)}[x_\alpha\binom{0\ m}{k\ j}/x^3]$. Combinations of sums like this multiply coupling terms that include first derivatives of Δ with respect to ionic displacements, e.g.,

$$\left[\frac{\partial^2}{\partial\Delta\begin{bmatrix} l \\ k \end{bmatrix}\partial\Delta\begin{bmatrix} l' \\ k' \end{bmatrix}}\Phi\right]\left[\frac{\partial}{\partial x\begin{bmatrix} m \\ j \end{bmatrix}}\Delta\begin{bmatrix} l \\ k \end{bmatrix}\right]\times\left[\frac{\partial}{\partial x\begin{bmatrix} m' \\ j' \end{bmatrix}}\Delta\begin{bmatrix} l' \\ k' \end{bmatrix}\right]. \quad (6)$$

The irregular behavior at the Brillouin-zone center can be traced to the Θ_α sums which, when Fourier transformed give

$$\Theta_\alpha(k,j;\mathbf{q})=\frac{4\pi i}{V}[1-\delta(\mathbf{q})]\sum_Q{}' \frac{Q_\alpha+q_\alpha}{|\mathbf{Q}+\mathbf{q}|^2}e^{-\iota(\mathbf{Q}+\mathbf{q})\cdot\mathbf{x}(k,j)}, \tag{7}$$

where $\mathbf{Q}$ is a reciprocal lattice vector and V is the volume of a unit cell. $\delta(\mathbf{q})$ is 1 for wave vectors that equal reciprocal lattice vectors, and zero otherwise. The $\mathbf{Q}=\mathbf{0}$ term clearly diverges in the limit $\mathbf{q}\to\mathbf{0}$, (but not at $\mathbf{q}=\mathbf{0}$) and gives rise to the anomalous behavior. $\delta(\mathbf{q})$ is a constant of integration that corresponds to the macroscopic field on sites k from a lattice of dipoles with unit charge at the j sites. This term prevents the infinities at $\mathbf{q}=\mathbf{0}$.

Cohen *et al.*[13] had an identical problem in their *ab initio* electron-gas model. In order to calculate frequencies at finite $\mathbf{q}$, they remove from (7) the shift of the potential due to lattice polarization induced by longitudinal phonons. The polarization shift is approximated by a Gaussian average, with a half-width on the order of the unit-cell dimension. To our experience, this approximation is a valuable tool in exploring the general shapes of the dispersion curves. However, this approximation produces small errors in the frequencies, and generates inaccuracies in certain thermodynamic functions that depend on higher-order derivatives of the spectrum. In particular, strain derivatives of the harmonic energy may be sensitive to the choice of the weighing function. Temperature derivatives of shear elastic constants thus depend on the choice of the Gaussian half-width.

For the calculation of unambiguous thermodynamic properties in an internally consistent model, we explicitly eliminate potential shifts due to uniform fields from the definition of the stabilizing field (5). We define the stabilizing potential as the potential difference between the site in question and the average of the potential at neighboring sites. We shall demonstrate that the modification preserves the expressions for finite deformation, and thus at the long-wavelength limit, the models are identical. Moreover, the modified model reduces to the original one at the Brillouin-zone boundary as well.

We define the stabilizing potential as follows:

$$2\Delta\begin{bmatrix} l \\ k \end{bmatrix}=P\begin{bmatrix} l \\ k \end{bmatrix}-\frac{1}{n}\sum_{\begin{bmatrix} l' \\ k' \end{bmatrix}}^{n} P\begin{bmatrix} l' \\ k' \end{bmatrix}, \tag{8}$$

where the primed indices denotes sites neighboring to $\binom{l}{k}$ and the summation is carried over the n nearest-neighbor sites. For deformations that do not generate uniform fields, this definition reduces to (5). This is the case for elastic deformation and infinite wavelength phonons in centrosymmetric structures.

To facilitate the comparison with the original uncorrected model for the limit $\mathbf{q}\to\mathbf{0}$, it is useful to consider the induced macroscopic field. In the long-wavelength limit, the macroscopic field is given by the field of a uniform distribution of dipoles. Solution of Poisson's equation yields the polarization field $(4\pi i/V)(q_\alpha/q^2)e^{-\iota\mathbf{q}\cdot\mathbf{x}(k,j)}$. This term should be subtracted from (7) at the limit $\mathbf{q}\to\mathbf{0}$. It is identical to the $\mathbf{Q}=\mathbf{0}$ term in (8) and thus eliminates the irregular behavior. This correction is not valid for short waves, yet it is a useful test for the consistency of other corrections with the original model at the Brillouin-zone center.

At Brillouin-zone boundaries, the induced fields alternate over interatomic distances, and therefore phonons do not generate spurious potential shifts. It follows that any consistent solution should reproduce the frequencies of the original model both at $\mathbf{q}=\mathbf{0}$ and at the Brillouin-zone boundaries.

Longitudinal eigenvalues based on (8) are indistinguishable from the results of the long-wavelength treatment of (5) for wavelengths between infinity and two unit cells, and are identical with the uncorrected model at Brillouin-zone boundaries. The prescription of Cohen *et al.*[13] yields generally good agreement with the long-wavelength and Brillouin-zone edge limits, although discrepancies of few wave numbers do appear.

The modification in the definition of Δ (5) requires some adjustments in the dynamical matrices. These are summarized in Appendix B.

Appendix C gives the expressions used for calculating thermodynamic properties in the quasiharmonic approximation. These thermodynamic functions are experimentally accessible manifestations of the anharmonicity, and serve as tests of the aptness of the model Hamiltonian in the quasiharmonic limit in modeling thermoelasticity of oxides.

IV. RESULTS AND DISCUSSION

A. Model parameters

Table I lists the model parameters. Note that b, R^0_{ox}, Q_{ox}, and n_{ox} (subscript: O^{2-}) are independent of the cation. We were not able to fix the self-energy parameters of O^{2-}. In particular, the self-energy parameter increases with the cation, or the number of electrons in the system. This seems to indicate that the neglect of cation breathing is not fully justified. Although even the heavy cations are tightly bound relatively to O^{2-}, small fractional changes in their energies amount to sizeable changes in the absolute energy.[19]

The cation radii are ordered in size corresponding to the number of electrons. Figure 1 shows a correlation between the model radii and values derived from self-consistent-field (SCF) *ab initio* calculations. The latter are the radii of spheres that contain all the ion's charge but half an electronic charge.[20] The almost linear correlation suggests that the potential parameters faithfully represent the essential physics of repulsion. The inclusion of electron-electron correlation in the SCF calculations would probably enhance the correlation with our radii (cf. Ref. 16).

We note that the self-energy is a measure of the coupling of the ion's orbitals with the crystal states. In the band picture, it is the bandwidth that measures that coupling. Figure 2 compares the models self-energies with results from first principles SCF band-structure calcula-

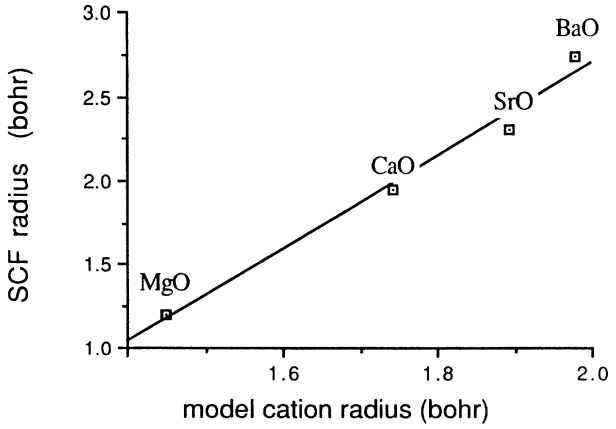

FIG. 1. Comparison between the model's cation radii and self-consistent-field radii (see text for further information).

tions of Bukowinski (Ref. 1) on MgO at a wide range of compressions. The high correlation suggests that the splitting of the local states due to the crystal environment is modeled reasonably. A similar correlation was obtained for the $B1$ (NaCl) phase of CaO. In both cases, the two energy measures are linearly correlated with compression. Although our self-energy expression (4) is not simply related to compression, these quantities correlate at the relevant range of pressures. This observation opens the possibility of sparing parameters in future work.

B. Phonon spectra

The calculated acoustic branch dispersion relations are in good agreement with neutron-scattering data (Figs. 3–6). The agreement for optical branches is generally poor, although the shapes of the dispersion curves are largely reproduced. Transverse optical (TO) branches for MgO agree well with the data, while the longitudinal

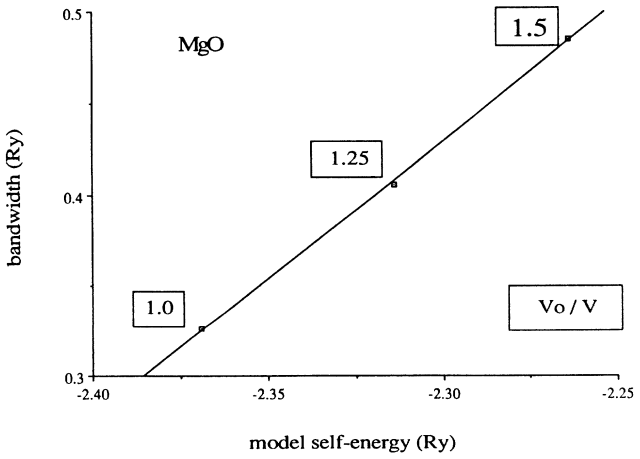

FIG. 2. Correlation between model self-energy and self-consistent-field valence bandwidth at various compressions for MgO. The bandwidth data is from Bukowinski (Ref. 1).

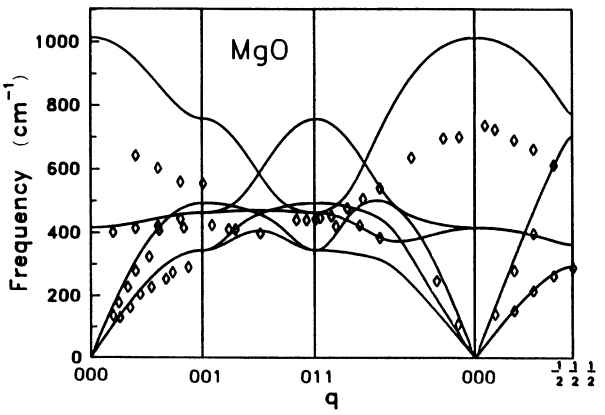

FIG. 3. Phonon-dispersion curves for MgO. The lines are calculated with the many-body Hamiltonian model. The diamonds are data from M. J. L. Sangster, G. Peckham, and D. H. Saunderson, J. Phys. C **3**, 1026 (1969); G. Peckham, Proc. Phys. Soc. **90**, 657 (1967).

(LO) are too high. The LO-TO splitting is reproduced for BaO, and the agreement worsens toward the lighter oxides. The LO-TO splitting is moderated by the charge relaxation.[11] The neglect of charge relaxation due to overlap may cause much of the discrepancy in our model. The problem becomes more acute for the smaller more electronegative cations. A similar trend, from heavy to light cations, was observed by Cohen *et al.*[13] in the PIB calculations. The fact that the discrepancy in LO-TO splitting is worse for MgO with the lowest cation polarizability suggests that in addition to ionic polarization, modifications in the many-body terms are needed for improved optical modes.

C. Quasiharmonic thermodynamics

The expressions for thermal properties in the quasiharmonic approximation are given in Appendix C. The harmonic free energy and its derivatives are obtained from the phonon spectra, which are computed at various configurations. Table II lists the calculated standard

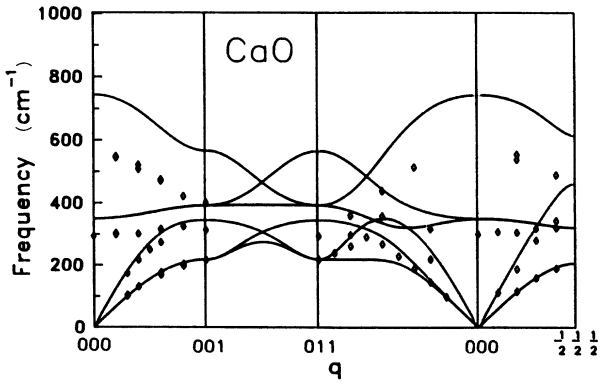

FIG. 4. Phonon-dispersion curves for CaO. The diamonds are data from Saunderson and G. E. Peckham, J. Phys. C **4**, 2009 (1970).

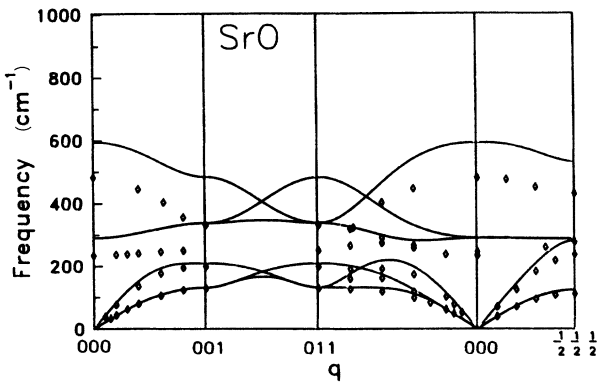

FIG. 5. Phonon-dispersion curves for SrO. The diamonds are data from K. H. Rieder, R. Migoni, and B. Renker, Phys. Rev. B **12**, 3374 (1975).

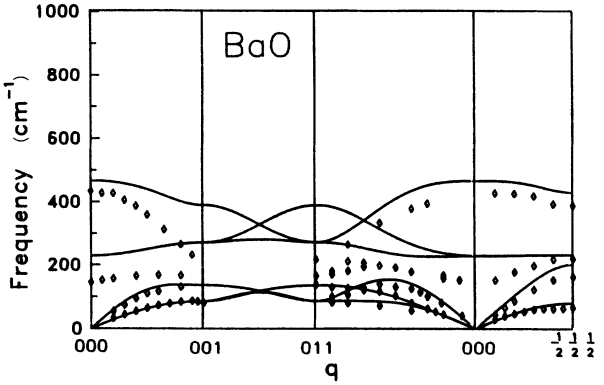

FIG. 6. Phonon-dispersion curves for BaO. The diamonds are data from S. S. Chang, C. W. Tompson, E. Gurmen, and L. D. Muhlstein, J. Phys. Chem. Solids **36**, 769 (1975).

temperature pressure (STP) thermoelastic properties along with published experimental data. The calculated heat capacities of MgO, CaO, and SrO are underestimated by up to 10%. The discrepancies diminish with the cation size, due to the better agreement of the phonon spectra (Figs. 3–5). Thus the calculated heat capacity of BaO agrees well with experiment, on par with the accurate spectrum (Fig. 6).

Noting that the only input on the fourth-order variation of Φ is the theoretical equation of state for CaO ($B1$) phase, the agreement between calculated and experimental anharmonic bulk properties is very satisfactory in most cases. The agreement for volumetric expansivity (α) is excellent for MgO and BaO, and reasonable for CaO and SrO. The product αK_T agrees very well with the data for all the compounds. The Grüneisen parameter (γ) agrees with the data within the experimental uncertainty. δ_S and δ_T (Appendix C) are reproduced very well for MgO, and progressively worse with increasing cation atomic number. This trend is correlated with the increasing anharmonicity (due to the low Debye temperature of the heavier compounds). The temperature derivative of α is not very well constrained experimentally. For MgO, where there is ample data, the calculated value is 10–15 % higher than observed. This is probably due to anharmonic effects, as shown below (discussion of Fig. 7). The derivative for CaO is more than 40% too high. It is expected that for CaO anharmonic effects are more significant, due to its lower Debye temperature.

The average volume derivatives of the elastic constants are in very good agreement with data for the four compounds (Ref. 9). It follows that the acoustic Grüneisen parameters are in good agreement with experiment.

Significant discrepancies appear for temperature derivatives of shear moduli B_S and B_{44}. Both moduli decrease rapidly with temperature. The quasiharmonic B_S in MgO vanishes at 700 K. This exaggerated temperature dependence may be due to a soft mode in the model. Negative eigenvalues, corresponding to instabilities, were encountered when the finite distortion that corresponds

TABLE II. Calculated and experimental thermodynamic properties at STP.

	γ	α (10^{-6} K^{-1})	δ_S	δ_T	C_P (J/mol K)	$(\partial\alpha/\partial T)_P$ (10^{-8}/ K^2)	αK_T MPa/K	$\partial K_S/\partial P$	q
MgO									
Calc.	1.66	31	3.2	6.0	33.9	7.3	5	4.2	1.7
Expt.[a]	1.53±.01	31	3.4±0.3	5.5	37.3	6.3±.3	5	4.2±0.3	1.6
CaO									
Calc.	1.64	34	3.2	5.6	40.0	5.5	3.8	4.1	1.7
Expt.[a]	1.6 ±1	38	4.8±0.8	6.5±1.1	43.3	3.0±1	3.7±0.5	5.4±6 4[b]	1.7
SrO									
Calc.	1.63	37	3.2	5.4	43.3	4.3	3.4	4.0	1.9
Expt.[a]	1.72±2[c]	42[c]	5.0±3.0	7.0±3.0	45.1		3.0±0.7	5.6±0.4	
BaO									
Calc.	1.68	38	3.6	3.8	46.0	3.8	3.0	3.6	3.3
Expt.[a]	1.48±0.15	38	5.6±2.6	7.5±3.0	45.4		3.6±0.3	5.5	

[a]From data compiled by Sumino and Anderson.
[b]Data $\partial K_T/\partial P$ taken from Ricet *et al.*
[c]Not including the entire range of a.

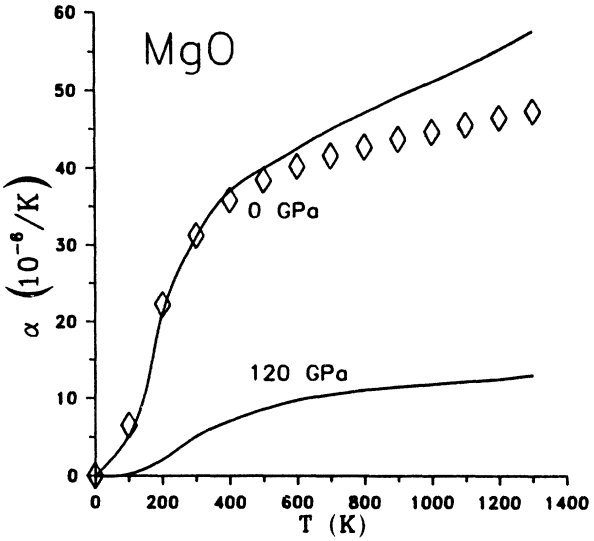

FIG. 7. The temperature dependence of the thermal expansivity calculated by the present model (line) and experimental (diamonds, data from Anderson and Suzuki).

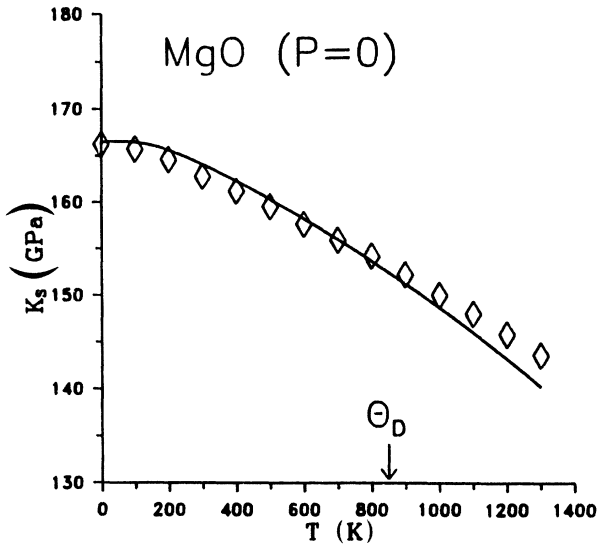

FIG. 8. The temperature dependence of the adiabatic modulus of MgO at zero pressure. The line is calculated by the present model. The diamonds denote data from O. L. Anderson and I. Suzuki, J. Geophys. Res. **88**, 3549 (1983).

to B_s (tetragonal) exceeded 0.01. Some of the discrepancy in the temperature derivatives of the elastic moduli can be attributed to anharmonic effects, that are likely to be large in the presence of a soft mode.

Calculation of shear moduli with the prescription of Cohen *et al.*[13] for the dynamic matrices (Sec. III B) reveals a significant dependence on the half-width of the Gaussian weighing function, particularly for B_s. A change of 50% in the half-width changes B_s by 40 GPa.

D. High pressure and temperature results for MgO

Figure 7 compares the calculated volumetric thermal expansivity with experimental data for MgO. The model reproduces the thermal expansivity to 400 K. At higher temperatures, the calculated temperature derivative is about three times higher than that observed. In Fig. 8 we plot the adiabatic bulk modulus of MgO to high temperatures. The calculated adiabatic bulk modulus agrees with the observations to 1000 K. Above this temperature [$\approx 1.1\times$(Debye temperature)], the predicted K_s is lower than that observed. This is probably due to the anharmonic contributions to the phonon spectrum, which we have neglected. Another source of error in the high-temperature range may be the LO frequencies, which are poorly predicted by the model. Figure 9 shows the temperature dependence of αK_T. Anderson and Suzuki[21] have calculated the thermal pressure directly from experimental data. Our calculations agree with theirs to 400 K. Above this temperature, Anderson and Suzuki find that the thermal pressure is independent of temperature, while we find a slight increase with temperature. The flattening of the experimental curve may be an anharmonic effect.

The model can predict high-temperature behavior of volume-dependent properties at pressures for which anharmonic effects are sufficiently suppressed. Laboratory data under simultaneous high pressure and temperatures are not extensive enough to allow systematic comparison with theoretical results. Seismic data, on the other hand, has enabled the recognition of trends in the behavior of acoustic properties with high pressure and temperature. Anderson[15] deduced from a large body of seismic observations on the acoustic response of the oxide Earth mantle that $[(\partial \ln V_s/\partial \ln V_p)]_P \approx 2-2.5$ where V_s and V_P are the shear (transverse) and compressional (longitudinal) wave velocities, respectively. He has attributed this to the different effect temperature has on the shear and bulk modulus. Partial melting is an alternative explanation to the high $[(\partial \ln V_s/\partial \ln V_p)]_P$, since V_s vanish

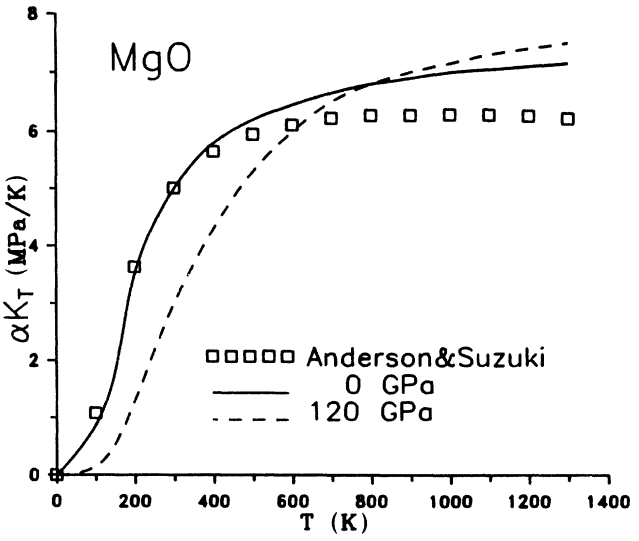

FIG. 9. The temperature dependence of αK_T at zero pressure. The line is calculated by the present model. The squares are experimental values by Anderson and Suzuki.

in any molten domain. For a subsolidus mantle, Anderson finds that the temperature dependence of the bulk modulus must be anomalously low. δ_s (defined in Appendix C) for relevant minerals is reduced from 3.9 ± 1.4 under laboratory conditions, to 1.4 ± 0.4 at compressions of 1.1–1.4.[22] The calculated pressure and temperature dependence of δ_s in MgO is presented in Fig. 10. Two isotherms are plotted, along with experimentally determined values at zero pressure. Our calculations indicate that compression indeed lowers δ_s by an amount that is consistent with the findings of Anderson (Ref. 15). This suggests that no partial melting is required to interpret the lower mantle seismic data.

For moderate compressions, the logarithmic isothermal volume derivative of the Grüneisen parameter $q=[(\partial \ln\gamma/\partial \ln V)]_T$ can be taken as a constant.[23] It is of interest to find the limits of this approximation, which is used in reduction of experimental data. Figure 11 shows the variation of γ and q with pressure for two isotherms. For a given pressure, γ is not very sensitive to temperature. Our model predicts a decrease in q with compression, as well as with temperature. This trend has been predicted independently for monatomic lattices.[24]

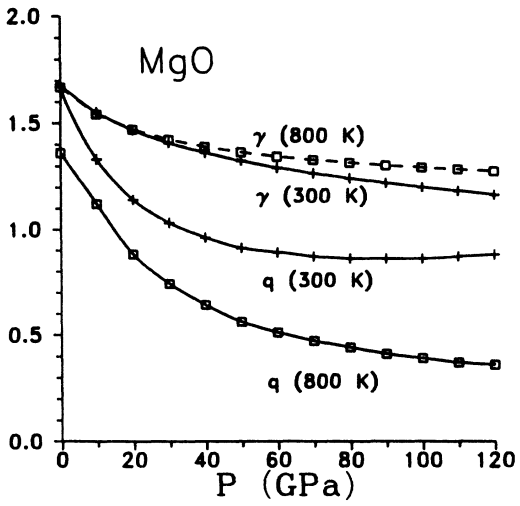

FIG. 11. Calculated pressure and temperature dependence of γ and q.

E. Phase transitions

Structural phase transformations in ionic solids pose stringent tests to ground-state energy theories. Recent advances in high-pressure experimental techniques enabled the documentations of $B1$-$B2$ (NaCl-CsCl) transition in the alkaline-earth oxides.[25] The nearest-neighbor static model calculations (Ref. 12) give accurate equations of state of the $B2$ (CsCl) phases of CaO and SrO, even though no data from these phases was used to constrain the parameters. Moreover, the predicted transition pressure was within 20% of the observed. The present study yields similar results. The introduction of second nearest neighbors increases the transition pressures by 2 GPa, and the vibrational correction to the Gibbs free energy decreased it by the same amount. The $B1$-$B2$ transition in MgO is predicted to occur at 500 GPa, beyond the range of current experiments.

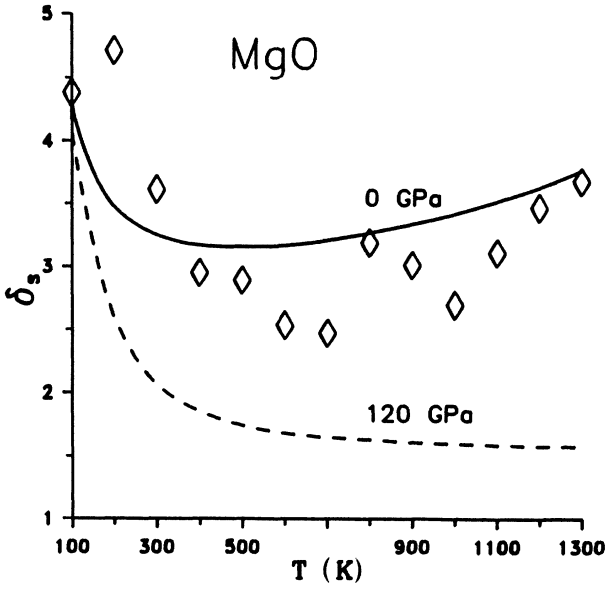

FIG. 10. The temperature and pressure dependence of the adiabatic Anderson-Grüneisen parameter. The lines are isobars calculated from the present model. The diamonds are from data, given by Anderson and Suzuki.

An interesting result of our calculation is that the $B2$ phase of CaO is elastically unstable below 34 GPa. This is consistent with the observation that the higher pressure phase is not quenchable.[17]

The ability of the model to predict the $B2$ phase equation of state and the close agreement with experimental phase stability data suggests that we can investigate the thermodynamic properties of the $B2$ phase. Table III lists the properties of the two phases at the transformation pressure (75 GPa in our model). Note the increase in the Grüneisen parameter and the thermal expansivity, and the decrease in the bulk velocity ($\sqrt{K_s/\rho}$ where ρ is the density).

It is interesting to compare the predictions of the many-body model with rigid-ion potentials. Based on central pair potentials calculations, Jeanloz and Roufosse[26] have predicted increases in γ and in α across a transition with such a density jump (10%). The central pair potentials predict a relative change of $\Delta\gamma/\gamma_{B1}\leq 0.3$, while the many-body model predicts 0.47. Both atomistic models differ from continuum models, which yield decreases in both α and γ.[26] Changes in acoustic velocity across phase transformations have particular significance in geophysics, where the distinction between phase transformation and chemical heterogeneity is crucial to modeling seismic data. The present many-body model yields a 2% decrease in the bulk velocity, which is the low end of the range predicted by pair potentials.[27]

TABLE III. Calculated thermodynamic properties across $B1$-$B2$ transformation in CaO.

	α (10^{-6} K^{-1})	$K_{s'}$	γ	δ_s	δ_T	$(\partial\alpha/\partial T)_P$ (10^{-8} K^2)	q	V_ϕ (m/sec)
$B1$	6.5	3.63	1.16	2.04	4.80	2.5	0.82	9371
$B2$	11	3.84±0.3	1.70	1.92	4.86	2.9	0.85	9115
($B1$-$B2$)/$B1$	0.69		0.46<					−0.02
	0.5<; <0.9[a]		0.19<; <0.32[a]					10<; <.02[b]

[a]Data taken from Jeanloz and Roufosse, 1982.
[b]Data taken from Jeanloz, 1983.

V. CONCLUSIONS

We have presented a parametric model that reduces the quantum mechanical picture of the oxide solid to a semiclassical ionic one. The model captures much of the intricate many-body effects by ascribing to each ion a single internal coordinate. The model parameters convey intuitive meaning to the physical constituents of the system.

The agreement between the calculations' predictions and experimental measurements is encouraging. The bulk thermodynamic properties are in excellent agreement with experiments to high temperatures. We cannot well predict the behavior of individual elastic constants under high temperature and compression. Some of the anharmonic parameters of the model are in very good agreement with data. While aggregate properties are the more important observables in applications such as geophysics and material engineering, our shortcomings in individual predictions underscore deficiencies in the model. The model attributes all the many-body interactions to the potential-induced breathing. Ionic polarization probably gives rise to some of the observed deviation from Cauchy relation, through modifications of neighbors' overlap. Since the parameters are determined by fitting to the elastic constants, a bias is introduced to the breathing parameters. The fact that electron-gas models with similar simplifications have generated almost identical trends in the phonon spectra indicates that these simplifications caused the inaccuracy in both cases. We stress, however, that the simplicity of the model has allowed us to address a variety of processes with a quantitatively successful outcome. It is unusual that a simple parametric model can represent such a variety of data as shear elasticity, phase stability, and optical properties, where 20 parameters suffice to describe four compounds.

A particularly promising aspect of the model is the ability to transport the parameters across phase transitions. The accurate prediction of $B2$ (CsCl-type) equation of state and stability field, when no data from this structure has been used, implies that the effects of environment on the internal state of O^{2-} have been modeled reasonably. This allows us to calculate changes of thermodynamic properties across the transformation with considerable confidence.

Although the model can benefit from improvements in the parametrization, as well as from incorporation of ionic polarization, it is already a workable tool, useful in predicting properties, as well as in illuminating observations and results of more fundamental studies.

The model generates thermodynamic properties of the cubic alkaline-earth oxides in good agreement with available data at STP. For MgO, where a large range in experimental temperatures is available, the model successfully predicts the temperature variation of the bulk modulus and thermal expansivity. Application to higher temperatures at zero pressure requires incorporation of anharmonicity. The calculations for simultaneously high pressure and temperatures are less sensitive to anharmonicity.

The model's predictions on the high-pressure behavior of thermoelastic parameters agree with certain interpretations of seismic data. High pressure suppresses the temperature dependence of the bulk modulus. This implies that no partial melting of the lower mantle is required to account for large values of $[(\partial \ln V_s/\partial \ln V_p)]_P$. The model predicts that the logarithmic volume derivative of the Grüneisen parameter increases with pressure. This conclusion is important for interpretation of experimental and seismic data.

ACKNOWLEDGMENTS

We wish to thank L. Stixrude for a thoughtful review of the manuscript. This research is supported by the Earth Science Program of the U.S. National Science Foundation (NSF).

APPENDIX A: EQUATION OF STATE AND ELASTIC CONSTANTS

The non-rigid-ion contribution to the static pressure is given by

$$P^{\rm nr} = -\left\{\frac{\partial}{\partial\Delta}\left[\frac{1}{2}\sum_{m,m',j,j'}{}' \phi\begin{bmatrix} m & m' \\ j & j' \end{bmatrix} + \sum_{m,j} S\begin{bmatrix} m \\ j \end{bmatrix}\right]\right\}\frac{\partial\Delta}{\partial V}, \tag{A1}$$

where V is the volume. Since Δ scales like an inverse length, its volume derivative is just $\Delta/3V$. The derivatives with respect to Δ can be expanded in terms of derivatives with respect to the ionic radii. From (3) it fol-

lows that

$$\frac{\partial R_k^l}{\partial \Delta\begin{bmatrix} l \\ k \end{bmatrix}} = -\frac{Q_k}{\Delta\begin{bmatrix} l \\ k \end{bmatrix}^2} . \tag{A2}$$

We differentiate Eq. (2) with respect to the ionic radii sum $R_{kk'}$ and substitute (A2) for their derivatives to obtain

$$\frac{\partial \phi\begin{bmatrix} l & l' \\ k & k' \end{bmatrix}}{\partial V} = -\frac{n_{kk'}}{3V}\frac{\phi\begin{bmatrix} l & l' \\ k & k' \end{bmatrix}}{R_{kk'}}\left[\frac{Q_k}{\Delta\begin{bmatrix} l \\ k \end{bmatrix}} + \frac{Q_{k'}}{\Delta\begin{bmatrix} l' \\ k' \end{bmatrix}}\right] . \tag{A3}$$

Similarly, differentiation of (4) yields

$$\frac{\partial S_k^l}{\partial V} = \frac{\sigma_k}{3VR_k}\left[\left(\frac{r_k^s}{R_k}\right)^2 - \frac{r_k^s}{R_k}\right]\frac{Q_k}{\Delta\begin{bmatrix} l \\ k \end{bmatrix}} . \tag{A4}$$

The elastic constants can be decomposed into energy contributions in accordance with the terms of Eq. (1), and a contribution from vibrations (superscript *TH*). In Voigt notation we may write

$$C_{ij} = C_{ij}^c + C_{ij}^\phi + C_{ij}^s + C_{ij}^{TH} , \tag{A5}$$

where each of i and j correspond to a pair of Cartesian coordinates. The Coulomb contribution C_{ij}^c is the same as in rigid-ion models.[28] The contribution to the elastic constants from the self-energy is

$$C_{ij}^s = \rho \sum_k \left[\frac{\partial^2 S_k}{\partial \Delta^2}\frac{\partial \Delta}{\partial \eta_i}\frac{\partial \Delta}{\partial \eta_j} + \frac{\partial S_k}{\partial \Delta}\frac{\partial^2 \Delta}{\partial \eta_i \partial \eta_j}\right] , \tag{A6}$$

where ρ is the mass density and η_{ii}, η_i are the strains. The summation is carried over all deformable ions. The contribution from short-range repulsion (2) contains the common rigid-ion terms, and the following many-body terms, and a mixed term:

$$C_{ij}^\phi = \rho \cdot \frac{1}{2}\sum_{l,l',k,k'}{}' \left[\left[\frac{\partial^2 \phi\begin{bmatrix} l & l' \\ k & k' \end{bmatrix}}{\partial \Delta^2}\frac{\partial \Delta}{\partial \eta_i}\frac{\partial \Delta}{\partial \eta_j} + \frac{\partial \phi\begin{bmatrix} l & l' \\ k & k' \end{bmatrix}}{\partial \Delta}\frac{\partial^2 \Delta}{\partial \eta_i \partial \eta_j}\right] + \frac{\partial^2 \phi\begin{bmatrix} l & l' \\ k & k' \end{bmatrix}}{\partial x \partial \Delta}\left[\frac{\partial \Delta}{\partial \eta_i}\frac{x_{\alpha j}x_{\beta_j}}{x} + \frac{\partial \Delta}{\partial \eta_j}\frac{x_{\alpha i}x_{\beta i}}{x}\right]\right] , \tag{A7}$$

where the indices of the Cartesian components are suppressed. The derivatives of $\Delta\binom{l}{k}$ with respect to strains have been evaluated by Ewald-transformed lattice sums. The second derivative of the ionic radius is readily given by

$$\frac{\partial^2 R_k^l}{\partial \Delta\begin{bmatrix} l \\ k \end{bmatrix}^2} = \frac{2Q_k}{\Delta\begin{bmatrix} l \\ k \end{bmatrix}^3} . \tag{A8}$$

In a stressed medium, acoustic waves propagate with velocities that are determined by effective moduli, which differ from C_{ij} by terms involving the initial stress.[28] For cubic crystals under hydrostatic pressure P, these are

$$B_{11} = C_{11} - P , \tag{A9}$$

$$B_{12} = C_{12} + P , \tag{A10}$$

$$B_{44} = C_{44} - P , \tag{A11}$$

and the pressure P is given by the volume derivative of Φ.

The shear constant C_s denotes $(C_{11}-C_{12})/2$, and $B_s = (B_{11}-B_{12})/2$.

APPENDIX B: DYNAMIC MATRICES

The prescription (6) for the stabilizing potential requires some modifications in the dynamical matrix derived by Cohen *et al.*[13] The dynamical matrix is defined as

$$D_{\alpha\beta}(j,j';\mathbf{q}) = (M_j M_{j'})^{-1/2} e^{-i\mathbf{q}\cdot\mathbf{x}(jj')} \times \sum_m e^{-i\mathbf{q}\cdot\mathbf{x}(m)} \Phi_{\alpha\beta}\begin{bmatrix} m & 0 \\ j & j' \end{bmatrix} , \tag{B1}$$

where M_j is the mass of ion in sublattice j and the couplings

$$\Phi_{\alpha\beta}\begin{bmatrix} m & 0 \\ j & j' \end{bmatrix} = \frac{\partial^2 \Phi}{\partial u\begin{bmatrix} m \\ j \end{bmatrix}\partial u\begin{bmatrix} 0 \\ j' \end{bmatrix}} \tag{B2}$$

are interionic force constants. The summation is carried out over all unit cells. The solution of the mechanical problem of harmonic free oscillations is given by diagonalizing (B1). The normal-mode frequencies are obtained from the square root of the eigenvalues.

The differentiation of $\Phi(x,\Delta)$ with respect to displacements generates rigid-ion-like terms from the dependence

on pair distances x, and additional terms with partial derivatives with respect to the stabilizing potential Δ. The second-order differentiation produces additional mixed derivatives.

The term involving second derivatives of the stabilizing potential with respect to mixed ionic displacements is of particular interest, as it controls the LO-TO (longitudinal-transverse optical) mode splitting (Boyer *et al.*, Ref. 11). This term replaces the charge product in the rigid-ion model. Since the stabilizing potential is proportional to the Madelung energy, it generates terms similar to the rigid-ion Madelung terms that, when grouped together, give rise to a modified effective charge (Cohen *et al.*, Ref. 13). In the present prescription, the stabilizing potential is proportional to the Madelung energy as well, but the grouping of terms is slightly different:

$$z_{kk'}=z_k z_{k'}+\frac{(c_k-c_{n\langle k\rangle})z_{k'}+(c_{k'}-c_{n\langle k'\rangle})z_k}{2} , \quad \text{(B3)}$$

where $n\langle k\rangle$ is the neighboring site of k, and following Cohen *et al.*

$$c_k=\sum_{l',k'}{}' \frac{\partial\phi\begin{bmatrix}0 & l'\\ k & k'\end{bmatrix}}{\partial P\begin{bmatrix}0\\ k\end{bmatrix}} . \quad \text{(B4)}$$

The primed sum in (B4) means that for $l'=0$ and $k=k'$ the derivative of the self-energy should be summed. In the case of a diatomic lattice, for $k\neq k'$, $Z_k=-Z_{k'}$, and the dynamical charge cross product (and hence the LO-TO splitting in the NaCl and CsCl structures) is not modified from Cohen *et al.* Cohen *et al.* (Ref. 13) defined a convenient lattice sum, the theta sum:

$$\Theta_\alpha(k,j;\mathbf{q})=\sum_m{}' e^{-i\mathbf{q}\cdot\mathbf{x}(m)}\frac{x_\alpha\begin{bmatrix}0 & m\\ k & j\end{bmatrix}}{x^3} \quad \text{(B5)}$$

that arises from first derivatives of the long-range electrostatic potential in a modulated lattice. This term has been factored out from all the dynamical matrix terms that include first derivatives of the stabilizing potential and second derivatives of Φ. In the present formulation, the derivatives of the stabilizing potential Δ are given as combinations of P [Eq. (8)], and thus the Θ sums are grouped to similar combinations:

$$\Theta^*_\alpha(k,j;\mathbf{q})=\frac{\Theta_\alpha(k,j;\mathbf{q})-\Theta_\alpha(n\langle k\rangle,j;\mathbf{q})}{2} , \quad \text{(B6)}$$

where Θ^* replaces Θ of the original formulation (Cohen *et al.*, Ref. 13). Note that unlike Cohen *et al.*,[13] in evaluating the Θ sums, we include both the direct and Fourier contributions to the Ewald-theta transformed sums. As $\mathbf{q}\rightarrow\mathbf{0}$, the individual Θ diverge but their differences, and hence Θ^*, approach zero—the proper limit—at $\mathbf{q}=\mathbf{0}$.

APPENDIX C: ANHARMONIC PROPERTIES

The thermodynamic properties of the lattice can be obtained from the quasiharmonic spectrum. In this approximation the Helmholtz free energy is given by[28]

$$F_H(\eta,T)=\sum_q [\tfrac{1}{2}h\nu_q(\eta)+kT\ln(1-e^{-h\nu_q(\eta)/kT})] , \quad \text{(C1)}$$

where ν_q is the frequency of mode q and the summation is taken over the Brillouin zone. h and k are the Planck and Boltzmann constants, respectively, and T is the temperature. Note that the frequencies are assumed to be a function of the configuration, as represented by the Lagrangian strain η. For isotropic deformations in cubic crystals we replace η by the volume V. The isothermal bulk modulus, is evaluated from

$$K_T=-V\left[\frac{\partial^2(\Phi+F_H)}{\partial V^2}\right]_T . \quad \text{(C2)}$$

In order to compute α, the volumetric thermal expansivity, we evaluate the product αK_T:

$$\left[\frac{\partial P}{\partial T}\right]_V=\left[\frac{\partial S_H}{\partial V}\right]_T=\alpha K_T . \quad \text{(C3)}$$

S_H is the entropy of the harmonic phonons, and is given by the temperature derivative of F_H. In the same way the quasiharmonic contribution to the heat-capacity at a given volume is simply

$$C_V=-T\left[\frac{\partial^2 F_H}{\partial T^2}\right]_V . \quad \text{(C4)}$$

The heat capacity at constant pressure is given by $C_p=C_V(1+\alpha\gamma T)$ where

$$\gamma=\frac{V\alpha K_T}{C_V} \quad \text{(C5)}$$

is the thermal Grüneisen parameter, which is evaluated from (C3) and (C4). The isentropic bulk modulus, obtainable from acoustic data, is computed from $K_s=K_T(1+\alpha\gamma T)$. The Anderson-Grüneisen parameter is the isobaric logarithmic volume derivative of the bulk modulus. For the adiabatic modulus it is given by

$$\delta_s=-(\alpha K_s)^{-1}\left[\frac{\partial K_s}{\partial T}\right]_P . \quad \text{(C6)}$$

---

*Present address: Earth Sciences Institute, The Hebrew University, 91 904 Jerusalem, Israel.

[1]M. S. T. Bukowinski, J. Geophys. Res. **85**, 285 (1980); K. J. Chang and M. L. Cohen, Phys. Rev. B **30**, 4774 (1984).

[2]M. J. Mehl, R. E. Cohen, and H. Krakauer, J. Geophys. Res. **93**, 8009 (1988).

[3]M. P. Tosi and F. G. Fumi, J. Phys. Chem. Solids **25**, 45 (1964); A. D. B. Woods, W. Cochran, and B. N. Brockhouse, Phys. Rev. **119**, 980 (1960).

[4]M. S. T. Bukowinski, J. Geophys. Res. **87**, 303 (1982).

[5]G. V. Gibbs, Amer. Mineral. **67**, 421 (1982).
[6]M. J. Mehl, R. J. Hemley, and L. L. Boyer, Phys. Rev. B **33**, 8685 (1986).
[7]U. Schroder, Solid State Commun. **4**, 347 (1966); M. J. L. Sangster, G. Peckham, and D. H. Saunderson, J. Phys. C **3**, 1026 (1970).
[8]M. P. Verma and R. K. Singh, Phys. Status Solidi **33**, 769 (1969); M. P. Verma and S. K. Agarwal, Phys. Rev. B **8**, 4480 (1973); S. D. Sanyal and R. K. Singh, Phys. Status Solidi **105**, 193 (1981); R. K. Singh and S. D. Sanyal, Phys. Status Solidi **113**, K23 (1982).
[9]A. Agnon and M. S. T. Bukowinski, Geophys. Res. Lett. **15**, 209 (1988).
[10]R. J. Gordon and Y. S. Kim, J. Chem. Phys. **56**, 3122 (1972); C. Mulhausen and R. J. Gordon, Phys. Rev. B **23**, 4880 (1980); R. E. Watson, Phys. Rev. **111**, 1108 (1953).
[11]L. L. Boyer *et al.* Phys. Rev. Lett. **54**, 1940 (1985).
[12]R. J. Hemley, M. D. Jackson, and R. G. Gordon, Phys. Chem. Minerals **14**, 2 (1987); G. H. Wolf and M. S. T. Bukowinski, in *High Pressure Research in Mineral Physics*, edited by M. H. Manghnani and Y. Syono (Terra Scientific, Tokyo, 1987), p. 313.
[13]R. E. Cohen, L. L. Boyer, and M. J. Mehl, Phys. Rev. B **35**, 5749 (1987).
[14]See, e.g., F. D. Stacey, *Physics of the Earth* (Wiley, New York, 1977); M. H. P. Bott, *The Interior of the Earth; its Structure, Constitution and Evolution* (Elsevier, Great Britain, 1982).
[15]D. L. Anderson, Phys. Earth Planet. Inter. **45**, 307 (1987).
[16]J. C. Slater, *The Self Consistent Field for Molecules and Solids* (McGraw-Hill, New York, 1974).
[17]J. F. Mammone, H. K. Mao, and P. M. Bell, Geophys. Res. Lett. **8**, 140 (1981); P. Richet, H-K. Mao, and P. M. Bell, J. Geophys. Res. **93**, 15 279 (1988).
[18]M. S. T. Bukowinski, Geophys. Res. Lett. **12**, 536 (1985).
[19]The Hartree-Fock energy of fifth-row atoms is typically 50 times larger than the corresponding second-row atoms.
[20]We computed these with the nonrelativistic code of F. Herman and S. Skillman, *Atomic Structure Calculations* (Prentice-Hall, Englewood Cliffs, NJ, 1963).
[21]O. L. Anderson and I. Suzuki, J. Geophys. Res. **88**, 3549 (1983).
[22]Here compression is defined as (ρ/ρ_0) where ρ is the density and the subscript 0 denotes an uncompressed state.
[23]See, e.g., R. W. Roberts and R. Ruppin, Phys. Rev. B **4**, 2041 (1970).
[24]G. H. Wolf and R. Jeanloz, Geophys. Res. Lett. **12**, 413 (1986).
[25]See, e.g., Y. Sato and R. Jeanloz, J. Geophys. Res. **86**, 11773 (1981); see also Ref. 17.
[26]R. Jeanloz and M. Roufosse, J. Geophys. Res. **87**, 10763 (1982).
[27]R. Jeanloz, *High-Pressure Research in Geophysics*, edited by S. Akimoto and M. H. Manghnani (Center for Academic Publications, Japan/Tokyo, 1983) p. 479.
[28]D. C. Wallace, *Thermodynamics of Crystals* (Wiley, New York, 1972).